Laser-beam deflection measurements and modeling of pulsed laser ablation rate and near-surface plume densities in vacuum

Peter L. G. Ventzek and Ronald M. Gilgenbach
Intense Energy Beam Interaction Laboratory, Nuclear Engineering Department, The University of Michigan, Ann Arbor, Michigan 48109-2104

David M. Heffelfinger[a] and Jeffrey A. Sell
Physics Department, General Motors Research Laboratories, Warren, Michigan 48090-9055

(Received 27 December 1990; accepted for publication 15 April 1991)

Quantitative measurements of ablated material from the surface of polyethyleneterephthalate (PET) by 248-nm excimer laser fluences up to 10 J/cm^2 are performed by HeNe laser-beam deflection in vacuum and by photoacoustic depth profiling in air. HeNe laser-beam deflection measures the density of gas phase material present in the ablation plume. Photoacoustic depth profiling is a nonintrusive diagnostic that directly measures the etch depths from laser ablation. A hydrodynamic model consisting of a centered rarefaction wave that reflects off the PET surface is shown to describe the laser deflection signals. From these measurements an estimate of the initial temperature of the ablated species is found.

I. INTRODUCTION

Laser ablation processing has important applications to etching of photoresist in electronics and laser ablative deposition of materials.[1] Our work focuses on the measurement of the mass removed per-ablating pulse by a new nonintrusive technique and on the temporal measurement of near-surface densities of the ablated material or ablation plume. We use complementary techniques both in vacuum and gas, based on the principle of laser-beam deflection through a refractive index gradient.[2–5]

First we use a laser-generated acoustic wave to measure the depth of the pit etched by pulsed laser ablation. When a pulsed laser irradiates a solid it is well known that an acoustic/shock wave is propagated through the solid.[6–8] At fluences below and slightly above the ablation threshold, an acoustic wave is also propagated from the surface to the gas background.[2–4,9] The acoustic wave is a density perturbation which also produces a perturbation in the index of refraction. Hence, the acoustic wave can be detected by deflection of a low-power cw HeNe laser. The increase in the time-of-flight of the acoustic wave from the receding surface gives the depth of the ablation pit.

Other methods of measuring the etch-pit depth are stylus profilometry[10] and scanning electron microscopy (SEM). Both suffer from the disadvantage that they are not *in situ* measurements. A quartz crystal microbalance has also been used for sensitive etch rate measurements.[11,12] However, in this case the quartz crystal is spin coated with the polymer and the technique is not applicable to other materials. Another method of measuring the etch depth nonintrusively is by femtosecond laser pulse optical ranging.[13] This method, however, involves an extremely complicated femtosecond laser system and the depth resolution is limited to roughly 5 μm. Mirage detection of thermal waves[14] as opposed to acoustic waves has been used to determine the depth profile of a piece of bakelite that was mechanically machined. Our technique uses acoustic wave deflection of a probe beam. Scanned photoacoustic microscopy (SPAM) uses acoustic waves that are detected by an ultrasonic transducer .[15] Previous transient photoacoustic monitoring of pulsed laser drilling[16] used acoustic detection not as a depth measurement but rather as an indicator of gross physical damage. Again, this work did not use laser-beam deflection to detect the acoustic waves but rather an ultrasonic transducer.

The second method we have investigated involves the detection of the deflection of the probe laser beam in a vacuum at various distances from the surface and deducing from them the near-surface densities of ablated material and mass of the gaseous material in the ablation plume. Previous experiments in vacuum have characterized the regime where the ablation plume has become collisionless or nearly collisionless (i.e., at distances greater than 1 cm from the target) by a variety of diagnostics including time-of-flight (TOF) measurements, emission and absorption spectroscopy, and charge collection. Most previous studies conclude that below 10 J/cm^2, the ablation of polymers results in the production of mostly neutral molecules or polymer fragments.[1] Walkup *et al.*[17] used a Michelson interferometer to measure the time dependence of the density of ablated species in vacuum at 2.5 mm above targets of polyimide and Al_2O_3. They found evidence of plasma formation with the Al_2O_3 target but found that neutrals were the primary product ablated from the polyimide target. Campbell *et al.*[18] have shown, using charge collection that a fractional ionization of 0.0005–0.001 is produced by irradiation of polyimide with 100–600 mJ/cm^2 at 308 nm. Mass spectroscopic studies[19,20] and emission spectroscopy[21] indicate that the expanding ablation plume is made

[a]Currently with Biorad Laboratories, Richmond, CA.

 0021-8979/91/020587-07$03.00

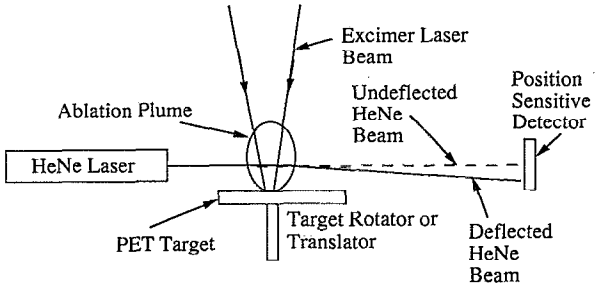

FIG. 1. Experimental configuration.

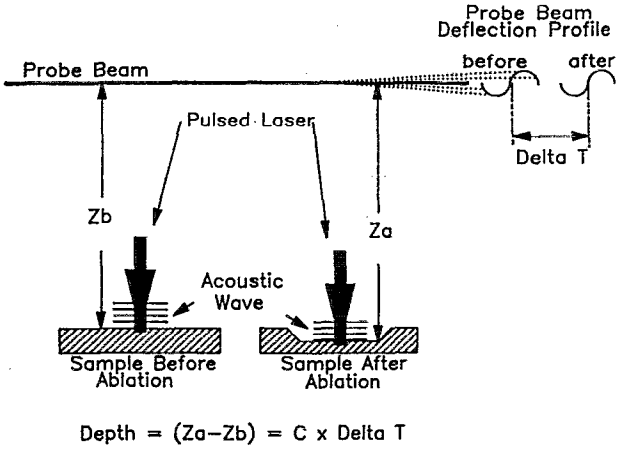

FIG. 2. Photoacoustic laser-beam deflection scheme for etch-pit depth measurement.

up of a fast and slow component. The faster component consists of material such as benzene whereas the slower component consists of heavier material (100 amu or higher). Visible emission spectroscopy by Koren and Yeh indicates that species such as C_2 are present in both mass waves.[21] At low fluences, 30–100 mJ/cm^2, Dyer and Srinivasan[22] performed time-of-flight experiments with a pyroelectric detector 7.5 cm from the target to determine a mean velocity of ablated species for PET and other polymers when they were ablated by 248-nm radiation. In this fluence range they found that the velocity increased approximately linearly with fluence from 2500 to 5000 m/s.

The present experiments and analysis for the vacuum case focus on the hydrodynamic regime very close to the surface (<4 mm), which is characterized by number densities that are within an order of magnitude of 10^{18}–10^{19} cm^{-3}.

II. EXPERIMENTAL CONFIGURATION

For the experiments conducted in atmospheric pressure air, a KrF excimer laser with a maximum pulse energy of 300 mJ was used. An ultraviolet (UV) sensitive detector monitored the timing of the KrF laser pulse. Laser deflection measurements were performed by passing a cw HeNe laser beam (probe beam) parallel to the target. For the photoacoustic depth profiling measurements, the HeNe beam was focused to a waist of 80 μm. The probe beam was incident on a fast position sensitive detector with a rise time of 25 ns.[23] Laser-beam deflection and timing signals were acquired on a Tektronix 2230 digital oscilloscope. The target-detector separation was approximately 0.25 m.

Figure 1 shows the experimental configuration for He-Ne laser deflection in vacuum. For these experiments, the ablation source was a pulsed beam of 248-nm radiation from a Lumonics KrF excimer laser with a maximum energy of 1.5 J/pulse and a pulse FWHM of 20 ns. The excimer laser beam was incident perpendicular to the target surface. The target was mounted on a translating vacuum feedthrough in a chamber which could be evacuated to 10^{-5} Torr. Unfocused, the maximum fluence was 200 mJ/cm^2. Focused, the average laser spot fluence could be increased to 10 J/cm^2. The fluence was varied by inserting quartz plates into the path of the ablating beam. An aperture was used to define the beam shape. The unfocused He-Ne probe beam was typically 1 mm from the surface. Laser deflection and timing signals were acquired on a fast oscilloscope. The distance of the detector from the sample was adjusted up to 1.55 m.

The target in these experiments was polyethyleneterephthalate (PET) commercially known as mylar.

III. EXPERIMENTAL RESULTS AND DISCUSSION: PHOTOACOUSTIC DEPTH PROFILING IN AIR

Figure 2 illustrates the approach used for photoacoustic depth profiling of laser ablated samples by accurately measuring the time it takes the acoustic pulse to travel from the surface to the HeNe probe beam. First, the PET is irradiated below its ablation threshold, at 14 mJ/cm^2, to generate a sound wave. This measures the surface position before the etch pit is created. Second, the surface is irradiated with a fluence above the ablation threshold, for the number of desired pulses, which creates the etch pit. Third, the PET is again irradiated below its ablation threshold, at 14 mJ/cm^2, to generate a sound wave. This provides a measurement of the surface position (etch pit) after laser ablation. The etch depth may therefore be calculated from the following:

$$d = c(\Delta t_a - \Delta t_b), \tag{1}$$

where d = etch-pit depth, c = speed of sound in the ambient medium (here, air), Δt = time between pump laser pulse and time that the sound pulse is detected, a = after ablating pulse, b = before ablating pulse.

The time for the acoustic wave to travel from the material surface to the HeNe probe beam was interpreted as the time between the excimer laser pulse and the zero crossing of the laser deflection signal. Figure 3 shows two laser deflection signals, one before ablation (that which crosses zero first) and one after ablation (that which crosses zero last). The time between the zero crossing of the two pulses is the measure of the etch depth. The differing amplitudes of the two traces in Fig. 3 are due to variations in the excimer pulse energy. For a single set of

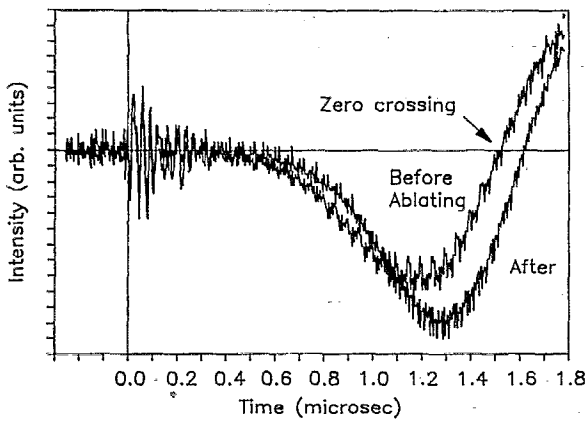

FIG. 3. Experimental data showing laser beam deflection signals due to acoustic waves acquired before and after ablation.

two pulses from the diagnostic laser, the minimum detectable time change of the zero crossing is 50 ns which corresponds to a minimum detectable etch depth of 17 μm. This depth resolution is a small fraction of the etch depth for a large number of accumulated pulses. Measurements of etch pits created at 1.2 J/cm^2 were repeated for different numbers of accumulated excimer laser pulses so that etch depth as a function of accumulated pulses could be obtained and compared with etch depths measured by cross-sectional optical microscopy. This comparison is presented in Fig. 4. The microscopy indicated that the etch pit was not sharp sided but rather more triangular in shape because of variations in the excimer laser pulse fluence across the spot. This explains the deviation of the photoacoustic results from the depth profile since photoacoustic depth profiling measurements tend to measure less than the maximum etch-pit depth: they measure an average pit depth because the acoustic wave is a superposition of many waves from different points in the pit. From the photoacoustic depth profiling an etch depth of 0.42 μm/pulse is measured. This compares very well with the 0.5 μm/pulse measured at the same fluence level by Lazare and Granier.[11] Also, Lazare and Granier[11] report the same ablation rate for PET at 248 nm in vacuum as in air.

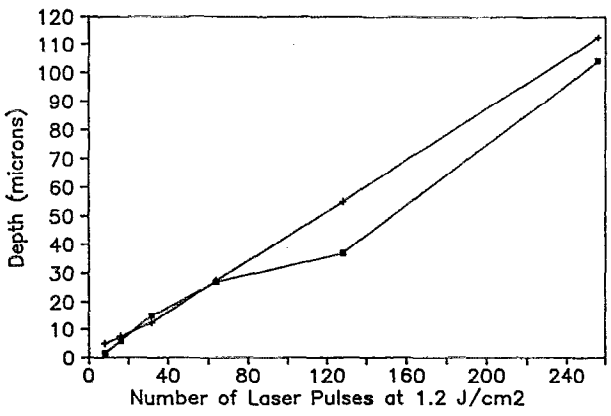

FIG. 4. Etch-pit depth vs number of laser pulses at 1.2 J/cm^2. Measurements by acoustic laser beam deflection (■) are compared to pit depths determined by cross sectional optical microscopy (+).

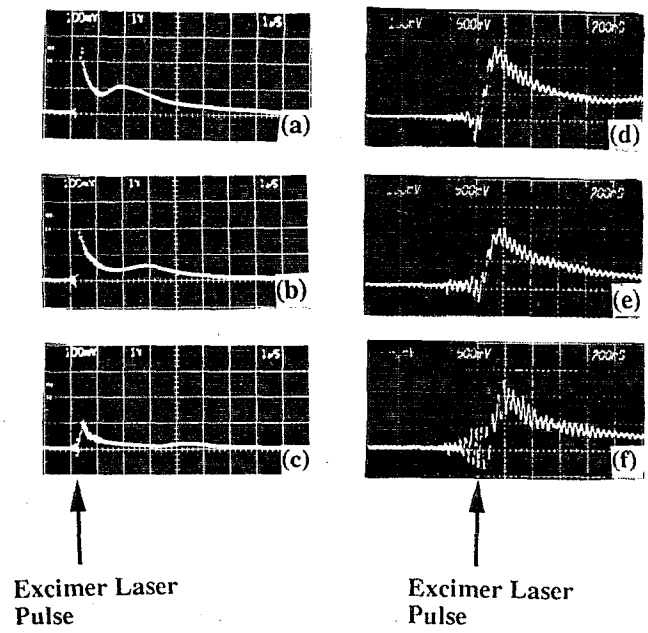

FIG. 5. Laser beam deflection signals in vacuum at various probe beam positions (0.5–2 mm) for two different time scales from 8 J/cm^2 of 248-nm radiation ablating PET. A positive signal corresponds to a deflection towards the PET sample surface. Time scales are 1 μs/div for (a), (b), and (c) and 200 ns/div for (d), (e), and (f). All traces are 100 mV/div except for (f) which is 50 mV/div. Probe beam positions are 0.5 mm for (a) and (d), 1 mm for (b) and (e), and 2 mm for (c) and (f).

IV. EXPERIMENTAL RESULTS AND DISCUSSION: QUANTITATIVE MEASUREMENTS OF LASER ABLATION IN VACUUM

Data in this section were obtained by the laser deflection system shown in Fig. 1. Figure 5 shows laser deflection signals for which the probe beam has been translated normal to the target surface between 0.5 and 2 mm. The laser fluence was approximately 8 J/cm^2 for each measurement. At high fluences (those greater than 3 J/cm^2) the deflection signal displays two peaks: a fast peak and a slow peak. At lower fluences, the laser deflection signals display only a single peak; the later peak disappears. The deflection system is oriented such that a positive signal is a deflection toward the PET sample surface. If the probe laser beam is being deflected by neutrals then the density of material is increasing toward the target surface; if the material were plasma then the deflection signal would indicate an electron density increasing away from the target surface. With most experimental evidence showing greater than 99% neutrals, it is likely that He-Ne deflection is from neutrals and the first peak is indicative of a signal that one would expect from the density profile of a neutral rarefaction wave. The second peak is likely the second mass component that has been suggested by Hansen[19,20] and Koren and Yeh.[21]

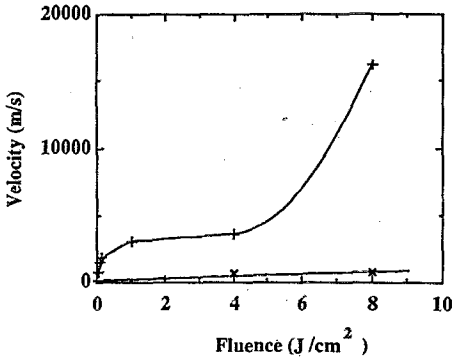

FIG. 6. Maximum deflection signal velocities for the fast peak (+) and the slow peak (×) as a function of laser fluence for 248-nm radiation incident on PET.

Figure 6 shows the velocity of the two peaks for different fluences. The position of these maxima have always been observed to be linear functions of time over the period they were observed (i.e., over distances of 3 mm and times of less than 1 μs for the fast peak and times less than 9 μs for the slow peak). The maximum velocity of the fast peak was 1.6×10^4 m/s at 8 J/cm^2 whereas the maximum velocity of the slow peaks were about an order of magnitude slower at 600–700 m/s. We observe, from 57 to 110 mJ/cm^2, that the average velocity, that which corresponds to the peak of the laser deflection signal, increases almost linearly from 900 to 1900 m/s. This compares with the 2500–5000 m/s observed by Dyer and Srinivasan using time-of-flight pyroelectric detection.[22]

Neutral particle density gradients are directly related to laser deflection signals by

$$\frac{d\rho}{dx}=\frac{\Delta\Phi/(K_nD)}{n_0}, \tag{2}$$

where $d\rho/dx$ = density gradient normal to the target surface, $\Delta\Phi$ = total laser beam deflection, K_n = Gladstone–Dale constant, n_0 = unperturbed index of refraction ≈ 1, D = pathlength of HeNe across target.

The Gladstone–Dale constant is a property of the species in the medium.[24] This constant can vary by as much as a factor of 5 with units of cm^3/molecule and by up to a factor of 2 with units of cm^3/g for species that are likely to be found in an ablation plume. Several species have been measured in previous ablation studies; benzene, water, C_2, and CO_2. Benzene has the largest K_n in both units. H_2O has the lowest K_n (cm^3/molecule) whereas CO_2 has the lowest K_n (cm^3/g). Since there are no exact data in these experiments on the material composition of the ablation plume, density gradients can only be specified from laser deflection data as lying within a range of values between those calculated using the properties of benzene, water, and CO_2. A selection of Gladstone–Dale constants for species that are likely in the ablation plume is found in Table I.

By varying the distance of the probe beam from the target as done for Fig. 5, a temporally and spatially varying

TABLE I. Molar refractivities and Gladstone–Dale coefficients at 632.8 nm for PET ablation products (Ref. 24). R_L is the Lorentz molar refractivity and R_G and K are the Gladstone–Dale constants.

Species	R_L cm^3/mol	R_L cm^3/g	R_G cm^3/mol	R_G cm^3/g	K cm^3/#
C_2	7.1	0.30	10.7	0.44	1.8×10^{-23}
CO_2	6.6	0.15	9.9	0.23	1.7×10^{-23}
C_6H_6	26.2	0.34	39.3	0.50	6.5×10^{-23}
H_2O	3.7	0.21	5.6	0.31	0.9×10^{-23}

description of the number density gradient of the gas-phase material ablated from the target can be obtained. Integrating the number density gradient over space at a particular time yields the number density as a function of position. With an additional integration, the number of molecules (or mass) of the ablation plume may be calculated. To perform the integration, it is assumed that the density approaches zero at the point where the density gradient approaches zero. Figure 7(a) shows a plot of number density gradient versus probe beam position calculated from laser

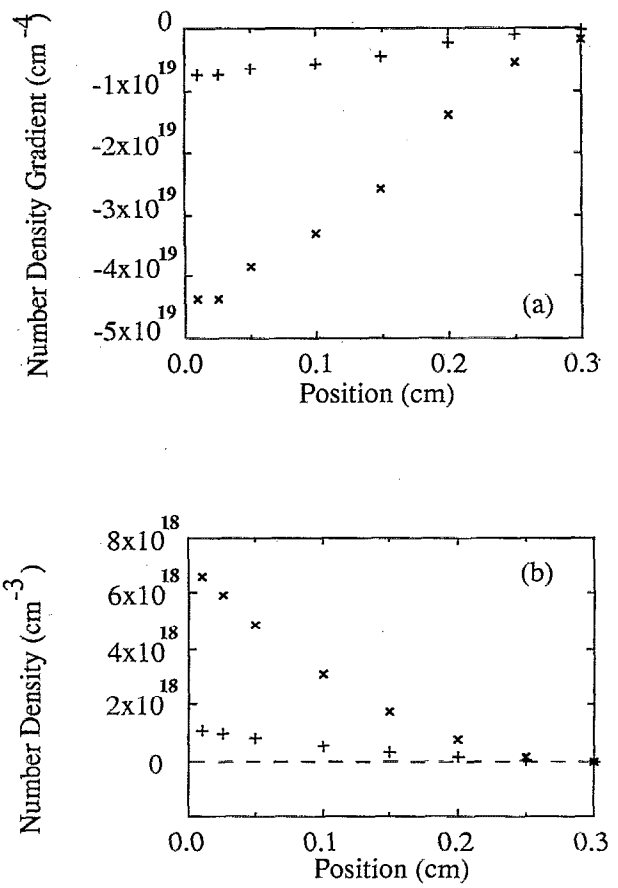

FIG. 7. (a) Density gradient and (b) density of ablated material 250 ns after excimer laser pulse of 8 J/cm^2. The number density gradient was calculated directly from a laser beam deflection signal using both benzene (+) and H_2O (×) as typical ablated species. Parabolic number density profiles were calculated from a straight-line fit of the density gradient. Zero corresponds to the point where the beam is 50% cut off by the surface.

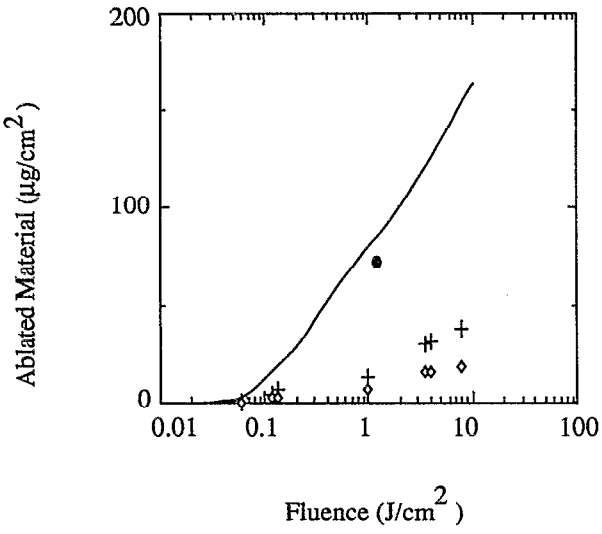

FIG. 8. Measured ablated material per unit area from PET as a function of excimer laser fluence determined by three different methods: photoacoustic depth profiling (●); data calculated by twice integrating the laser deflection signal vs position data assuming benzene as a typical species (◇) and CO_2 as a typical species (+); and quartz crystal microbalance data of Lazare and Granier (Ref. 11) (solid line).

deflection data (using benzene and water as model species) for a fluence of 8 J/cm^2 at 250 ns after the pulse. At 250 ns the density gradient approaches zero at 3 mm; we assume then that the density approaches zero at 3 mm. Integrating the density gradient in Fig. 7(a) yields the density as a function of position presented in Fig. 7(b). Note that the peak number densities (6.5×10^{18} cm^{-3} for benzene and 1×10^{18} cm^{-3} for water) are close to STP number density, 2.66×10^{19} cm^{-3}. A further integration yields number of molecules per unit ablated area present in the plume.

The procedure described above was repeated at several fluences, from around 50 mJ/cm^2 to 8 J/cm^2, yielding a plot of ablation plume mass per unit area versus fluence assuming in one case that all the species are benzene and in the other extreme (this refers to the relative magnitudes of R_G for benzene and CO_2) that all the species are CO_2. The plot of ablation plume mass per unit area for fluences above the ablation threshold between 0.05 and 10 J/cm^2 is presented in Fig. 8. The data of Lazare and Granier[11] and the mass removed, calculated using photoacoustic depth profiling are also presented in Fig. 8 for comparison.

Laser deflection ablation plume mass measurements are significantly lower than those measured using a quartz crystal microbalance or photoacoustic depth profiling. The discrepancy arises because the last two diagnostics directly measure total ablated mass, however the ablation plume mass calculated by laser deflection in vacuum is a measure of gaseous species only. Laser deflection measurements in vacuum do not detect material ablated from the PET surface in particulate form. Thus, the difference in the measurements indicates that a large fraction of the material is particulate in nature. Particulate matter was observed by us as a deposit on the sample around the ablation region and visually from scattered light from the HeNe beam. Srinivasan *et al.*[25] have used gel-permeation chromatography to characterize the particulate ejected from polymethylmethacrylate (PMMA). Debris has also been observed by von Gutfeld and Srinivasan[26] using electrostatic collection.

V. MODELING OF LASER ABLATION IN VACUUM

The near-surface hydrodynamics of laser ablation in a vacuum can be modeled by a centered rarefaction wave described by the equation:

$$\frac{\rho}{\rho_0}=\left[1-\left(\frac{\gamma-1}{\gamma+1}\right)\frac{1}{c_0}\left(c_0+\frac{x}{t}\right)\right]^{2/(\gamma-1)}, \tag{3}$$

where ρ = gas density, ρ_0 = initial gas density, γ = ratio of specific heats, c_0 = initial speed of sound of the material.

For this expression, x less than zero corresponds to a region of uniform density at $t=0$; x greater than zero corresponds to a region of vacuum at $t=0$. At times greater than zero, the laser ablation causes material from $x<0$ to expand into the region $x>0$. The point $\rho=\rho_0$ moves to the left (i.e., in the direction of negative x) at c_0. This model fails when the point $\rho=\rho_0$ collides with the unablated solid surface. At this time, the density near the solid surface will begin to decrease (to conserve mass). A first estimate for a model of the expansion of material into vacuum would be to set the point where $\rho=\rho_0$ as stationary. While this is satisfactory for a steady-state ablation source, it is not adequate to describe a pulsed laser ablation source.

For pulsed laser ablation, a more appropriate model is that of the case in which a centered rarefaction wave reflects off a wall.[27,28] We have sought a numerical solution to the equations that describe the adiabatic motion of a gas: the adiabatic equation of state, continuity equation, and momentum conservation equation. Using the adiabatic condition:

$$P=K\rho^{\gamma}, \tag{4}$$

where P = pressure, K = a constant, ρ = density, and γ = ratio of specific heats.

One can transform the continuity and momentum conservation equations to two partial differential equations in c and u:

$$\frac{\gamma-1}{2}c\frac{\partial u}{\partial x}+u\frac{\partial c}{\partial x}+\frac{\partial c}{\partial t}=0, \tag{5}$$

$$\frac{2}{\gamma-1}c\frac{\partial c}{\partial x}+u\frac{\partial u}{\partial x}+\frac{\partial u}{\partial t}=0, \tag{6}$$

where c is the local speed of sound and u is the fluid velocity.

The equation of state is

$$\frac{\rho}{\rho_0}=\left(\frac{c}{c_0}\right)^{2/(\gamma-1)}, \tag{7}$$

where the subscript 0 corresponds to an initial value.

The Warming–Kutler–Lomax method (W-K-L),[29] used for the solution of Burgers' equation, was used to

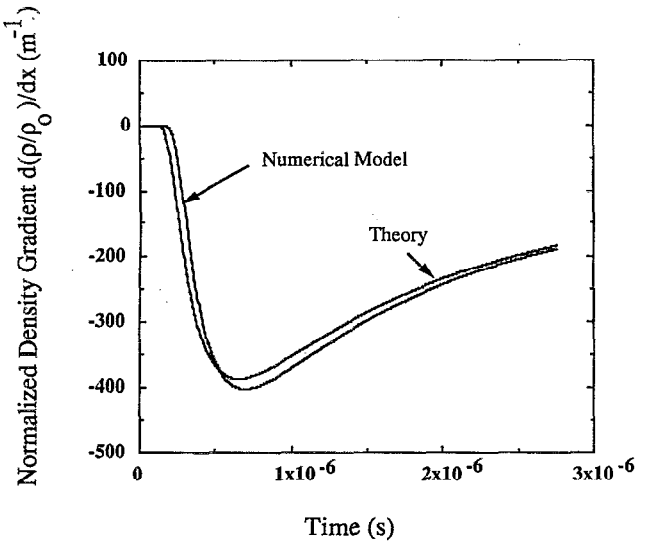

FIG. 9. Computer model benchmark comparison with the case of a centered rarefaction wave. The case presented is $\gamma = 1.4$, $c_0 = 650$ m/s, $F = 3$, $\omega = 2.7$ and spatial meshes of 50 μm.

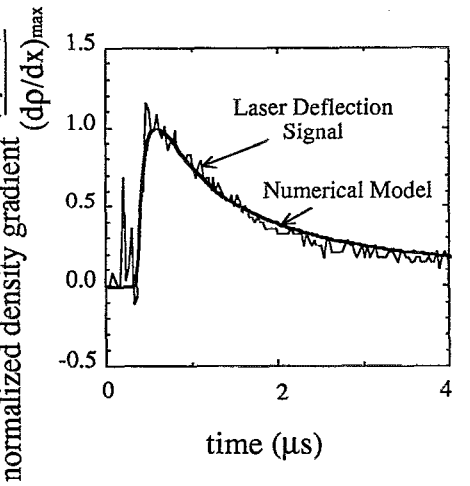

FIG. 10. He-Ne laser beam deflection signal for a probe-PET sample surface separation of 1 mm. The fluence for this case was 1 J/cm^2. A computer simulation (smooth line) of a centered rarefaction wave that reflects off the target surface is presented for comparison with the experimental data. Simulation parameters are: c_0, initial sound speed, 650 m/s; γ, the ratio of specific heats, 1.4. The spatial mesh size was 50 μm. Both the experimental data and the simulation results are normalized to 1.

solve Eqs. (5) and (6). At the target surface, a reflecting boundary condition is used. If the wall is chosen as the boundary between the $i = 1$ and $i = 0$ mesh, then one sets the speed of sound c at mesh 1 and mesh 0 (on both sides of the reflecting boundary), to be equivalent; further, one sets the fluid velocity u at meshes 0 and 1 to be equal and opposite. The initial sound speed and fluid velocity are specified. The sound speed was given a constant value c_0 from the surface of the target to a mesh i_{max} beyond which it was set to 0. The fluid velocity was set to zero from 1 to i_{max}. Beyond i_{max}, the fluid velocity was set to $2c_0/(\gamma - 1)$ which is the hydrodynamically fastest fluid velocity; to insure stability, the fastest allowable velocity was set to this value. Using Eq. (7), the sound speed, normalized to its initial value, can be related to the normalized density. As a benchmark of the computer model, the case of a centered rarefaction wave [Eq. (3)] was modeled. Figure 9 presents the normalized density gradient calculated by the computer model and from equation 3 for $\gamma = 1.4$, $c_0 = 650$ m/s, $F = 3$, $\omega = 2.7$ and a spatial mesh of 50 μm. The initial position of the rarefaction wave was 2 mm. The density gradient is shown for $x = 2.5$ mm.

Figure 10 shows a laser deflection signal with the probe beam 1 mm from the surface for a fluence of 1 J/cm^2 and compares it with the computer model simulating a centered rarefaction wave that reflects off a wall. The numerically generated curve is normalized to 1 and the experimental data is normalized such that the average peak value is 1. Agreement was sought that would minimize the square of the error between the normalized curves by varying c_0 for a fixed γ. The initial sound speed that provides the best agreement with experimental data is 650 m/s. The ratio of specific heats γ chosen is 1.4 (γ benzene = 1.45 at 25 C and 1 atm). For this case we have used a mesh size of 50 μm and an initial density region constant over 50 μm. The ratio of the spatial mesh to the time step was $[2c_0/(\gamma - 1)]/F$, where F was typically 3. The parameter ω in the W–K–L method was set to 2.7.

The computer model predicts the linear relation between the peak deflection signal and position which was observed in Fig. 6. Figure 11 shows the magnitude of the peak density gradient predicted by the numerical model (combined with etch depth data) and laser deflection measurements at 1 J/cm^2. The model gradients were calculated assuming that all the ablated species were benzene and that they were equally distributed over a 50 μm thickness after the laser pulse. Lazare shows that at 1 J/cm^2 the etch depth is 0.48 μm. Using a density of PET of 1.4 g/cm^3, one can calculate a ρ_0 of 1×10^{20} cm^{-3} at distances less than 50 μm. The experimental peak gradients are consistently

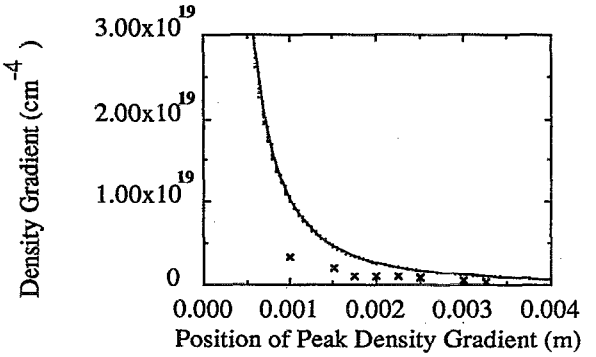

FIG. 11. Magnitude of peak density gradient predicted by the numerical model (solid line) compared with peak density gradients calculated from laser deflection data assuming a typical ablation plume species is benzene ($\times$). The model gradients were calculated assuming the benzene was uniformly distributed over 50 μm after the laser pulse.

lower than the model predicts. Again, this discrepancy is caused by the fact that laser deflection through an ablation plume expanding into vacuum does not measure particulate ejected from the surface.

Having estimated c_0 for a given γ from the reflected rarefaction wave model, one can infer the initial temperature of the ablated species given an assumed typical ejected molecular mass. The speed of sound is

$$c=(\gamma kT/m)^{1/2}, \tag{8}$$

where k = Boltzmann constant, T = initial temperature of ablated species, c = speed of sound, m = molecular mass of the ablated species.

We have assumed that a typical ejected ablated species was benzene, giving the initial temperature of 3000 K. Data on the pyrolysis of benzene indicate that it would be stable over the few μs interval in which our data are recorded.[30]

VI. CONCLUSIONS

Photoacoustic laser beam deflection has been demonstrated to be an effective method for measuring the depth of craters formed by pulsed UV laser ablation in gas environments. The method is not extendable to vacuum but is effective at pressures as low as 2 Torr, below which the signal is too low to measure; the speed of sound is dependent only on the temperature and not the pressure. This technique is, however, extendable to the case of a liquid instead of a gas above the sample making the technique useful for chemically assisted laser etching or biomedical applications such as tissue ablation. This technique is applicable to all materials and is nondestructive since no contact is made with the sample. Good agreement between the mass removal rate in air measured by photoacoustic depth profiling and with previous measurements by quartz crystal microbalance was found.

Laser-beam deflection in a vacuum was also used to measure the mass of expanding ablated gas-phase material. The masses calculated by this method were consistently lower than the previous measurements of total ablated mass by Lazare and Granier[11] and by our photoacoustic measurements. This mass deficit is caused by the fact that the laser deflection measurements in vacuum do not measure particulate material ablated from the surface. A hydrodynamics model consisting of a reflected centered rarefaction wave was developed which shows good agreement with the experimental beam deflection signal in a vacuum and also gives an estimate of the initial ablation species temperature.

ACKNOWLEDGMENTS

This research was supported by the National Science Foundation (Grant No. ECS-8351837), Los Alamos National Laboratory and an equipment gift from the Bonisteel Foundation.

[1] J. T. C. Yeh, J. Vac. Sci. Technol. A **4**, 653 (1986).
[2] J. A. Sell, D. M. Heffelfinger, P. Ventzek, and R. M. Gilgenbach, Appl. Phys. Lett. **55**, 2435 (1989).
[3] P. L. G. Ventzek, R. M. Gilgenbach, J. A. Sell, and D. M. Heffelfinger, J. Appl. Phys. **68**, 965 (1990).
[4] J. A. Sell, D. M. Heffelfinger, P. L. G. Ventzek, and R. M. Gilgenbach, J. Appl. Phys. **69**, 1330 (1991).
[5] G. Chen and E. S. Yeung, Anal. Chem. **60**, 864 (1988).
[6] A. C. Tam, Rev. Mod. Phys. **58**, 381 (1986).
[7] G. Gorodetsky, T. G. Kazyaka, R. L. Melcher, and R. Srinivasan, Appl. Phys. Lett. **46**, 828 (1985).
[8] P. E. Dyer and R. Srinivasan, Appl. Phys. Lett. **48**, 445 (1986).
[9] G. E. Jamieson and G. C. Wetsel, Jr., *Optical-Beam-Deflection Probing of Blast Waves Near Solid Surfaces*, in *IEEE 1985 Ultrasonics Symposium*, edited by B. R. McAvoy (IEEE, New York, 1985).
[10] R. Srinivasan and B. Braren, J. Polymer Sci. **22**, 2601 (1984).
[11] S. Lazare and V. Granier, Laser Chem. **10**, 25 (1989).
[12] S. Lazare, J. C. Soulignac, and P. Fragnaud, Appl. Phys. Lett. **50**, 624 (1987).
[13] D. Stern, W. Z. Lin, C. A. Puliafito, and J. G. Fujimoto, Invest. Opth. Visual Sci. **30**, 99 (1989).
[14] D. Fournier and A. C. Boccara, in *Scanned Image Microscopy*, edited by E. A. Ash (Academic, London, 1980).
[15] Y. H. Wong, in *Scanned Image Microscopy*, edited by E. A. Ash (Academic, London, 1980).
[16] C. E. Yeack, and R. L. Melcher, Appl. Phys. Lett. **41**, 1043 (1982).
[17] R. E. Walkup, J. M. Jasinski, and R. W. Dreyfus, Appl. Phys. Lett. **48**, 1690 (1986).
[18] E. E. B. Campbell, G. Ulmer, B. Hasselberger, and I. V. Hertel, Appl. Surf. Sci. **43**, 346 (1989).
[19] S. G. Hansen, J. Appl. Phys. **66**, 1411 (1989).
[20] S. G. Hansen, J. Appl. Phys. **66**, 3329 (1989).
[21] G. Koren and J. T. C. Yeh, J. Appl. Phys. **56**, 2120 (1984).
[22] P. E. Dyer and R. Srinivasan, J. Appl. Phys. **66**, 260 (1989).
[23] C. L. Enloe, R. M. Gilgenbach, and J. S. Meachum, Rev. Sci. Instrum. **58**, 1597 (1987).
[24] W. C. Gardiner, Y. Hidaka, and T. Tanzawa, Comb. Flame **40**, 213 (1981).
[25] R. Srinivasan, B. Braren, R. W. Dreyfus, L. Hadel, and D. E. Seeger, J. Opt. Soc. Am. B **3**, 785 (1986).
[26] R. J. von Gutfeld and R. Srinivasan, Appl. Phys. Lett. **51**, 15 (1987).
[27] R. von Mises, *Mathematical Theory of Compressible Fluid Flow* (Academic, New York, 1958), p. 155.
[28] R. Kelly, Nucl. Instrum. Methods B **46**, 441 (1990).
[29] D. A. Anderson, J. C. Tanehill, and R. H. Pletcher, *Computational Fluid Mechanics and Heat Transfer* (Hemisphere, New York, 1984), pp. 148–149.
[30] J. H. Kiefer, L. J. Mizerka, M. R. Patel, and H.-C. Wei, J. Phys. Chem. **89**, 2013 (1985).